Neurochemistry International 128 (2019) 196–205

Contents lists available at ScienceDirect

Neurochemistry International

journal homepage: www.elsevier.com/locate/neuint

Reduced postnatal expression of cochlear Connexin26 induces hearing loss and affects the developmental status of pillar cells in a dose-dependent manner

Le Xie[a,1], Sen Chen[a,1], Kai Xu[a], Hai-Yan Cao[c], An-Na Du[d], Xue Bai[a], Yu Sun[a,**], Wei-Jia Kong[a,b,*]

[a] Department of Otorhinolaryngology, Union Hospital, Tongji Medical College, Huazhong University of Science and Technology, Wuhan, 430022, China
[b] Institute of Otorhinolaryngology, Tongji Medical College, Huazhong University of Science and Technology, Wuhan, 430022, China
[c] Department of Ultrasound, Union Hospital, Tongji Medical College, Huazhong University of Science and Technology, Wuhan, 430022, China
[d] Centre of Instrumental Analysis and Metrology, Wuhan Institute of Virology, Chinese Academy of Sciences, Wuhan, 430071, China

ARTICLE INFO

Keywords:
Connexin26
pillar cell
GJB2
Hearing loss
Development
Supporting cell

ABSTRACT

Mutations in the *GJB2* gene (which encodes Connexin26 (Cx26)) are the most common cause of non-syndromic deafness. Previous studies showed that an extensive knockout of the *Gjb2* gene in cochlear epithelium can cause severe deafness, significant hair cell (HC) loss and failure of pillar cells (a type of supporting cell, PCs) to differentiate in mice. This study aimed to establish different mouse models with gradient reductions of cochlear Cx26 expression and to investigate the effect of different reduced levels of cochlear Cx26 expression on hearing and development of PCs. According to the reduction in the levels of cochlear Cx26, these models were named high knockdown (KD), middle KD and low KD group. In the low KD group, the mice showed normal hearing and well-developed PCs. In the high KD group, up to 90 percent of supporting cells (SCs) lost Cx26 expression. These mice exhibited severe deafness, rapid hair cell degeneration and juvenile PCs. In the middle KD group, nearly half of SCs lost Cx26 expression. However, these mice showed a moderate deafness and a late-onset hair cell loss. Moreover, nearly all the PCs in mice of this group were in a partially differentiated state. These results indicated that reduction of postnatal expression of cochlear Cx26 induces hearing loss in a dose-dependent manner. Null Cx26 in a few SCs affects the developmental status of PCs and the hair cell degeneration pattern. The abnormal developmental status of PCs may be a potential cause of *Gjb2*-related hearing loss.

1. Introduction

Congenital sensorineural hearing loss (SNHL) stands out as the most common neonatal sensory disorder, with an incidence of approximately 1.4 per 1,000 newborns screened (July 21, 2017). In more than half of neonates with congenital SNHL, the cause is attributed to genetic factors (Rennels and Pickering, 2005). Mutations in a gene called *GJB2* (encoding Connexin26 (Cx26)) account for around a quarter to a half of hereditary cases of SNHL in different countries (Gazzaz et al., 2005; Liu et al., 2002; Rabionet et al., 2000; Tsukada et al., 2010). The Cx26 assembles with Connexin30 or with itself to form gap junctions in cochlear supporting cells (SCs) or fibrocytes, which can then facilitate intercellular communication between adjacent cells (Crispino et al., 2011; Harris, 2001; Sun et al., 2005). Two common mutations of the *GJB2* gene–35delG and 235delC–are found in European and Asian populations, respectively (Chan and Chang, 2014). These *GJB2* mutations result in truncating variants of Cx26 protein that lose their function completely (Azaiez et al., 2010).

Most of conditional Cx26-null mouse models display severe hearing loss at all frequencies, in which cochlear Cx26 was extensively knocked out in embryonic day or early postnatal day (Chen et al., 2014a, 2014b; Cohen-Salmon et al., 2002; Crispino et al., 2011; Sun et al., 2009; Wang et al., 2009). However, the direct cause of this deafness is still obscure (Jagger and Forge, 2015). Generally, hearing loss in the above models can be attributed to a significant loss of sensory hair cells in the middle and basal turn (Cohen-Salmon et al., 2002). However, the residual hair cells in the apical turn can survive for a few months, and this cannot explain why hearing impairment at low frequencies is also quite serious

* Corresponding author. Department of Otorhinolaryngology, Union Hospital, Tongji Medical College, Huazhong University of Science and Technology, Wuhan, 430022, China.
** Corresponding author.
E-mail addresses: sunyu@hust.edu.cn (Y. Sun), entwjkong@hust.edu.cn (W.-J. Kong).
[1] These authors contributed equally to this work.

https://doi.org/10.1016/j.neuint.2019.04.012
Received 18 March 2019; Received in revised form 17 April 2019; Accepted 19 April 2019
Available online 26 April 2019

(Chen et al., 2014b; Sun et al., 2009). In conditional Cx26-null mouse models, further investigations indicated that the developmental arrest of supporting cells occurs prior to the death of hair cells in all turns of the cochlea (Wang et al., 2009). Additionally, our previous study proved that this developmental arrest of the organ of Corti was mainly attributed to the deformities of pillar cells (a type of SC, PCs) and Deiter's cell (a type of SC coupled with an outer hair cell, DCs) (Chen et al., 2018a). Whether developmental arrest of PCs or DCs is another potential cause of hearing loss or an incidental phenomenon that does not affect hearing is an important question that remains to be answered.

Although there is no treatment based on the mechanism of *GJB2*-related hearing loss, some progress has been made with regard to gene therapy for reconstitution of cochlear Cx26 expression using a viral vector *in vivo*. Lin's group reported that hair cell loss can be greatly reduced and functional recovery of gap junction-mediated coupling among SCs is observed following viral-mediated reconstitution of cochlear Cx26 expression in conditional *Gjb2* knockout mice. However, there is no improvement in hearing (Yu et al., 2014). Another study showed that a 20–30 dB improvement was found at a specific frequency after similar *Gjb2* gene transfer in another Cx26-null mouse model. However, quantitative data of cochlear Cx26 expression before and after gene transfer are still lacking in this research (Iizuka et al., 2015). One potential explanation is that the difference in therapeutic effects between the above studies may be due to the differences in the amount of Cx26 re-expression in mouse cochlea. Therefore, there are two questions that must be answered first. (1) What is the minimum amount of cochlear Cx26 expression that can maintain the survival of auditory hair cells? And (2) Is there a minimum amount of cochlear Cx26 expression that can maintain normal hearing? In other words, whether there is a dose-dependent relationship between hearing loss and the amount of Cx26 deletion should be studied preferentially. Additionally, these two studies reported that the development of PCs can be partially restored by exogenously-expressed Cx26. Therefore, whether the development of PCs depends on the expression of cochlear Cx26 in a dose-dependent manner should also be explored.

According to previous studies, modulation of tamoxifen (TMX) dose can successfully control Cre activation (Erdmann et al., 2007; Hayashi and McMahon, 2002; McGovern et al., 2017). By using the Cre-LoxP system, cochlear Cx26 expression can be manipulated by changing the dose of TMX injection in a conditional Cx26-null mouse model. In this study, three different Cx26 knockdown (KD) mouse models (the low KD, middle KD and high KD groups) were established, and the expression of residual Cx26 showed successive decreases. We investigated the degrees of hearing loss and patterns of hair cell loss in these models. Additionally, the developmental status of PCs was carefully compared. This provided a better understanding of the effects of different amounts of cochlear Cx26 expression on hearing, survival of auditory hair cells and postnatal development of PCs.

2. Results

2.1. Establishment of models with different levels of Cx26 knockdown

To induce different reductions in the postnatal expression level of cochlear Cx26, mice were administered TMX by injection with 0.6 mg (low KD group), 1.1 mg (middle KD group) or 1.6 mg (high KD group) per 10g body weight. Radial sections were cut to show the residual Cx26 expression at P7. In the low KD group, most SCs in the cochlea and a few fibrocytes in the lateral wall still showed punctual signal of Cx26 protein (Fig. 1B, F and J). In the middle KD group, scattered Cx26-null SCs were observed in the cochlear epithelium, but most cells in the lateral wall had lost Cx26 signal (Fig. 1 C, G and K). In the high KD group, most SCs and fibrocytes showed no Cx26 expression (Fig. 1 D, H and L). In comparison with the control group, levels of Cx26 expression in the cochlear epithelium in the low, middle and high KD groups were 57.5 ± 3.7%, 38.8 ± 5.5% and 29.8 ± 6.0%, respectively (Fig. 1 M and N).

2.2. Residual Cx26 expression patterns and quantification of Cx26-null cells in the cochlear epithelium from different experimental groups

According to a previous study, almost all SCs in the cochlear epithelium expressed Cx26 at P7 (Zhang et al., 2005). To better understand the residual Cx26 expression in the cochlear epithelium, flattened preparations were used and Cx26-null cells were quantified in different turns of cochleae at P7. In the control group, Cx26 signals (red) were observed on the boundaries of PCs or DCs (Fig. 2 A, E and I). In the low KD group, scattered PCs or DCs had lost Cx26 expression and these Cx26-null cells were distributed evenly within the organ of Corti (Fig. 2 B, F and J). The number of Cx26-null PCs or DCs in the middle KD group was obviously greater than that in the low KD group (Fig. 2 C, G and K). Obviously, typical mosaic deletion pattern of cochlear Cx26 was observed in the low and middle KD groups. In the high KD group, most of the PCs or DCs had lost Cx26 signals (Fig. 2 D, H and L). Quantification of the results showed that the proportions of Cx26-null SCs (including PCs and DCs) were 33.9 ± 6.5%, 27.1 ± 2.1% and 23.5 ± 0.9% in the apical, middle and basal turns, respectively, of the low KD group (n = 5). These proportions in the middle KD group (n = 5) were 56.5 ± 3.9%, 48.6 ± 3.4 and 42.4 ± 3.8%, respectively. Moreover, approximately 90% of SCs had lost Cx26 expression in the high KD group (Fig. 2 M, n = 3). Quantification of Cx26-null PCs revealed that similar results in these groups. In the low KD group, the proportion of Cx26-null PC did not exceed 39.2%. However, 48.0–55.2% of PC had lost Cx26 expression in the middle KD group, while up to 85% of PCs did not express Cx26 in the high KD group (Fig. 2 N). (*$P < 0.05$, one-way ANOVA).

2.3. Distinct patterns of hearing loss in the different experimental groups

The auditory brainstem responses (ABRs) of all mice were measured at P20 and P60. Mice in the low KD group showed normal hearing at P20 and P60. At P20, the hearing thresholds in the middle KD group at 4, 8 16 and 32 kHz were 73.9 ± 3.4, 52.2 ± 4.3, 40.0 ± 5.3 and 52.8 ± 4.8 dB SPL, respectively (Fig. 3 A). The mean thresholds in the high KD group were high at around 80 dB SPL (Fig. 3 A). For adult mice at P60, the thresholds in the middle KD group at 4, 8 16 and 32 kHz were 80.0 ± 1.9, 64.3 ± 5.6, 43.6 ± 6.2 and 57.1 ± 7.1 dB SPL, respectively (Fig. 3 B). At this time, there was still no significant hearing loss in the low KD group (Fig. 3 B). Differences between the middle KD and the control group were significant at 4, 8 and 16 kHz at P60 (*$P < 0.05$, one-way ANOVA).

2.4. Morphological changes in different experimental groups

Resin sections were prepared for morphologic studies (9-12 sections from 3 to 4 mice in each group). The structures of organs of Corti in the control and low KD groups showed no significant pathological changes in any of the turns (Fig. 4 A–F). The tunnel of Corti (TC) was opened up and the Nuel's space (NS) was well formed in these two groups. However, malformed organs of Corti with closed TC (black arrow, Fig. 4 J–L) and NS were observed in all turns of the high KD group. After careful measurements, we found that the height of the organ of Corti in the middle KD group ($P < 0.01$, one-way ANOVA) or high KD group ($P < 0.01$, one-way ANOVA) was reduced in apical turn (Fig. 4 N). These parameters were also reduced in middle and basal turn of the middle KD or high KD group. Moreover, some organs of Corti degenerated totally in the middle turn of the high KD group (data not shown). However, no substantial spiral ganglion neuron loss was observed in these experimental groups (Fig. 4 M and O).

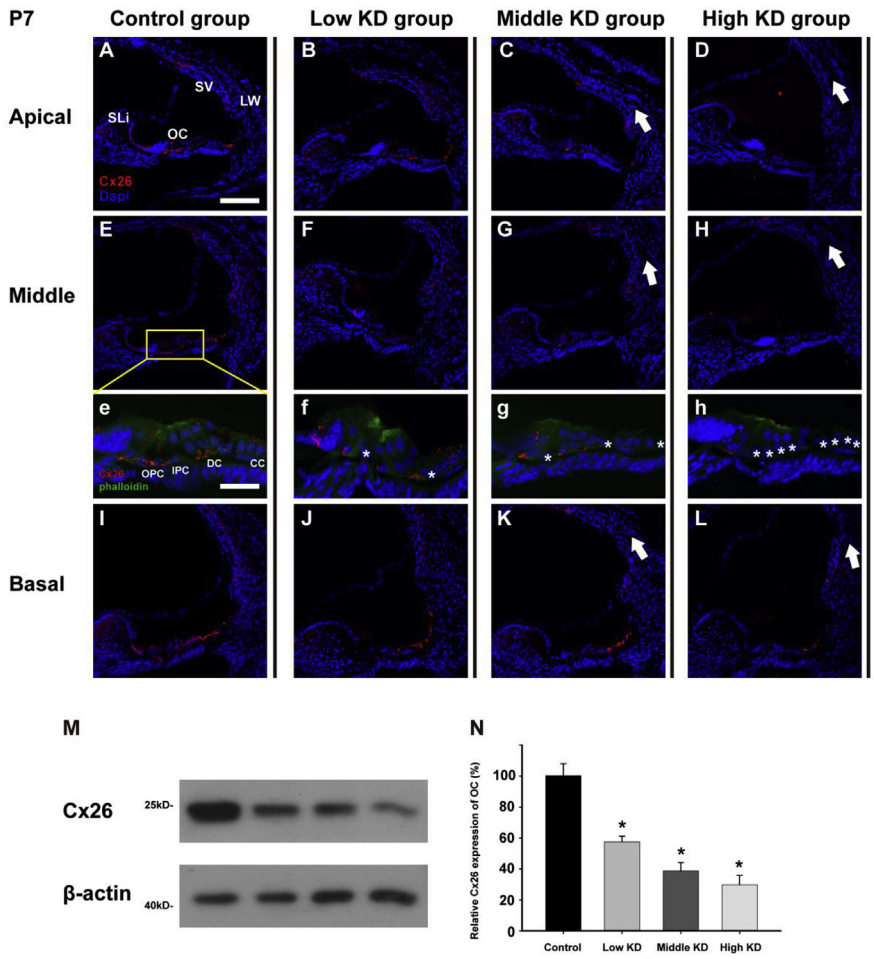

Fig. 1. Connexin26 expression in different Cx26 knockdown groups. (A, E and I) Immunolabelling of Cx26 (red) in apical (A), middle (E) and basal turns (I) of the control group; Parallel images of immunolabelling of Cx26 (red) in the low KD (B, F and J), middle KD (C, G and K) and high KD group (D, H and L); (e, f, g and h) Magnified images of the organ of Corti in the middle turns from the corresponding experimental groups (E, F, G and H); (M and N) western blot (M) and histogram (N) showing Cx26 expression in the cochlear epithelium of control and different experimental groups at P7 (n = 4 in each group). * indicates Cx26-null cells (e, f, g and h). OC, organ of Corti; SV, stria vascularis; SLi, spiral limbus; LW, lateral wall; CC, Claudious cell. The scales in panel A and e represent 100 and 40 μm, respectively. *$P < 0.05$, significantly different from control group (N).

2.5. Ultrastructural changes of supporting cells in the different experimental groups

The organs of Corti were observed at P20 by transmission electron microscopy (9-12 sections from 3 to 4 mice in each group). The opening of the TC was not affected and the phalangeal processes of the DCs were well developed (white arrow, Fig. 5 B) in the low KD group. A smaller organ of Corti with a fine structure was found in the middle KD group (Fig. 5 C). In accordance with previous studies, the TC could not open up and a hypertrophic phalangeal process (white arrow, Fig. 5 D) was observed between two outer hair cells (OHCs) in the high KD group. Moreover, the density of microtubules in IPCs or OPCs was reduced in this group (Fig. 5 K and L). In contrast, the fine phalangeal processes of DCs were well formed in the low and middle KD groups (white arrow, Fig. 5 B, C). Additionally, bundles of microtubules were observed in the bodies of IPCs and OPCs from the low or middle KD group (Fig. 5 F, G, J and K). The red and blue lines in Fig. 5 B represent the length of IPCs or OPCs, respectively. Compared with control, the relative lengths of IPCs and OPCs were reduced to 92.0 ± 2.0% and 79.8 ± 2.3%, respectively, in the middle KD group ($P < 0.01$, one-way ANOVA). In the high KD group, these parameters were reduced to 77.8 ± 1.2% and 67.1 ± 0.8%, respectively ($P < 0.01$, one-way ANOVA). Although no significant deformities were found in the middle KD group, the nuclei of OPCs and IPCs were closer together, which resulted in a smaller space of TC in this group (Fig. 5 Q and R). In comparison with controls, the relative distance between the nuclei of IPCs and OPCs was reduced to 79.7 ± 2.9% ($P < 0.01$, one-way ANOVA, 30 pairs of PCs from 3 mice, Fig. 5 T). The nuclei of OPCs and IPCs in the high KD group were next to each other (Fig. 5 D).

2.6. Distinct hair cell loss patterns in the different experimental groups

At P20, no substantial hair cell loss was found in the low or middle KD groups (Fig. 6 A–F). However, a significant cellular degeneration of hair cells and neighbouring SCs was observed in the middle turn from the high KD group (Fig. 6 J and G, n = 3). Moreover, scattered losses of OHCs or inner hair cells (IHCs) were found in the basal turn of the high KD group (white arrows, Fig. 6 K). At the same time, some pyknotic nuclei of OHCs were observed in basal turns from the high KD group (white arrowheads, Fig. 6 K). At P60, loss of a few OHCs was observed in the basal turn from the middle or low KD groups (white arrows, Fig. 6 M and N). However, the proportion of OHC lost in the low KD group was much less than that in the middle KD group (Fig. 6 O, n = 3–4). No obvious IHC loss was observed in the middle and low KD groups.

2.7. No significant reduction of DPOAE and No substantial ultrastructural changes of IHC was found in the middle KD group

The CtBP2 immunostaining (green) was performed to show the pattern of ribbon synapses in IHC of control and the middle KD group at P20 (Fig. 7 A). Quantification results (42 IHCs from 3 mice in each group) showed that there was no significant difference of the number of ribbon synapses per IHC between control and the middle KD group (14.69 ± 3.37 in control group and 15.26 ± 3.50 in the middle KD group, Fig. 7 B). The DPAOE input/output plots measured from control and the middle KD group were indistinguishable from each other at 8 kHz (Fig. 7 C) and 16 kHz (Fig. 7 D). Although the DPAOE levels of control group were slightly higher than those of the middle KD group at some input levels, their differences were not statistically significant

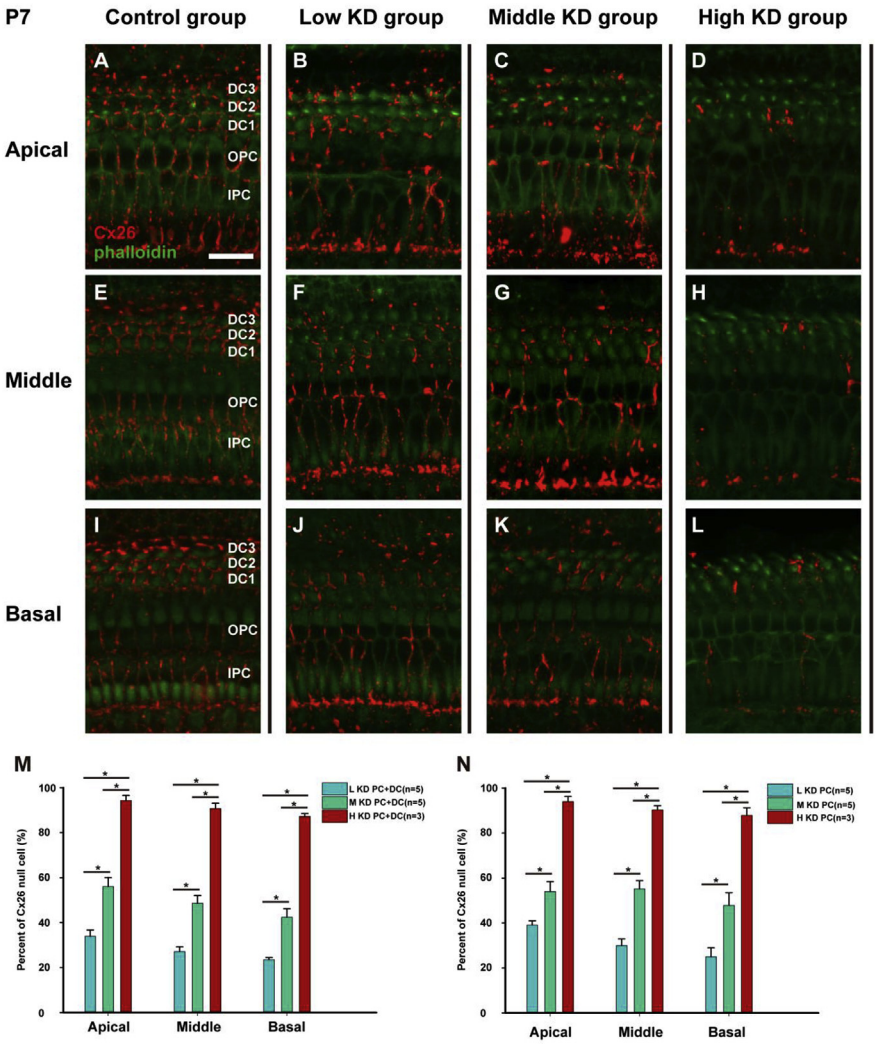

Fig. 2. Residual Cx26 expression patterns and quantification of Cx26-null cells in different experimental groups at P7. (A, E and I) Immunolabelling of Cx26 (red) in flattened preparations of apical (A), middle (E) and basal turns (I) from the control group (n = 3 in each group); Parallel pictures of Cx26 immunolabelling (red) in the low KD group (B, F and J), middle KD group (C, G and K) and high KD group (D, H and L); (M) Quantification of the total number of Cx26-null pillar cells (PCs) and Deiter's cells (DCs) in the different experimental groups (n = 3–5 in each group); (N) Quantification of Cx26-null pillar cells in the different experimental groups. The scale in panel A and represent 30 μm $^{*}P < 0.05$, significantly different from two groups.

($P > 0.05$, n = 5–6 mice in each group, unpaired *t*-test). Additionally, there was no representative pathological changes in IHC from the middle KD group (Fig. 7G and H). No signs of karyopyknosis, karyorrhexis or autophagy were observed in IHC or OHC (data not shown) from the middle KD group at P20.

3. Discussion

Different reductions in the postnatal expression of cochlear Cx26 result in varying degrees of deafness. To imitate the situation in humans with truncating variants of Cx26 protein, Cx26-null mouse models were previously established in which the *Gjb2* gene was widely knocked out in the inner ear. Although there were some small differences in knockout patterns, the Cx26 in the different types of SCs was almost completely lost. Accordingly, the knockout resulted in severe deafness in these models (Chen et al., 2014b; Cohen-Salmon et al., 2002; Crispino et al., 2011; Iizuka et al., 2015; Sun et al., 2009). In our study, the proportion of Cx26-null SCs was 42.4%–56.5% in the middle KD group. The mice in this group showed moderate hearing loss which was maintained into adulthood. Moreover, the proportion of Cx26-null SCs in the apical turn was about 10% higher than that in the basal turn in the middle KD group. This could explain why hearing loss at low frequencies is a little greater than that at high frequencies. When the proportion of Cx26-null SCs was less than approximately 35% in the

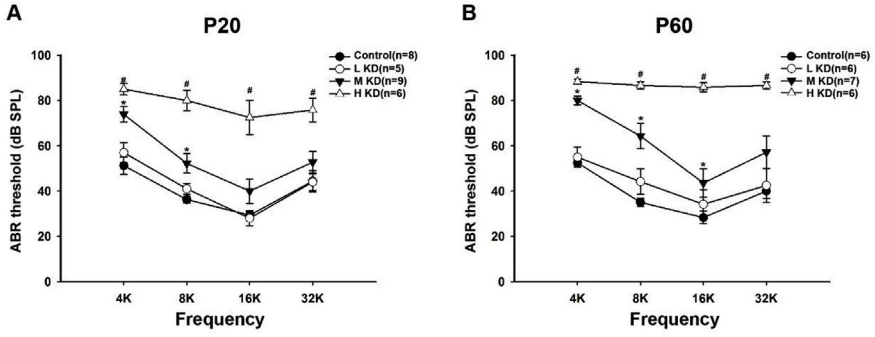

Fig. 3. ABRs in the different experimental groups at P20 or P60. (A) Hearing thresholds of control and different experimental groups at P20; (B) Hearing thresholds of control and different experimental groups at P60. # or * $P < 0.05$, significantly different from control group. L KD, low KD group; M KD, middle KD group; H KD, high KD group.

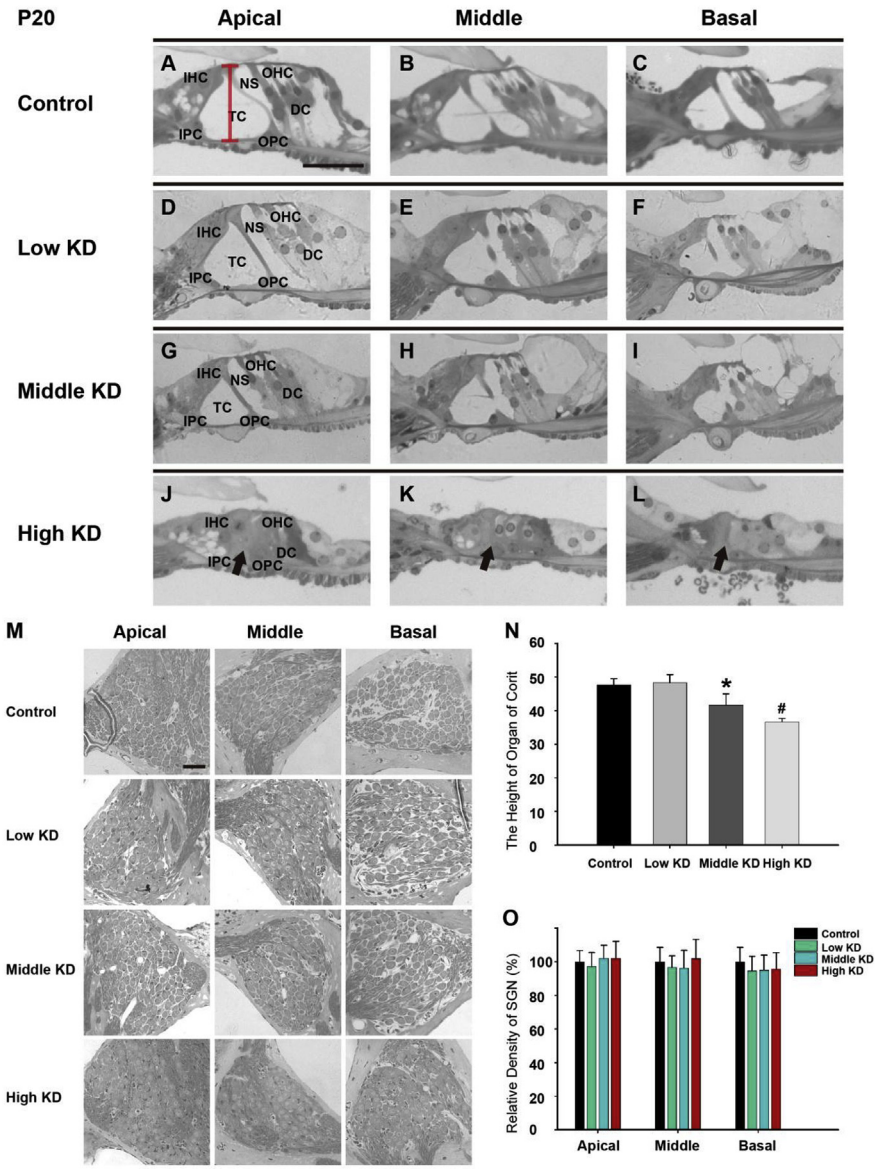

Fig. 4. Cochlear morphology in control and different experimental groups. (A, B and C): Morphology of the organ of Corti in apical (A), middle (B) and basal turns (C) from the control group; Parallel images of the organ of Corti in the low KD (D, E and F), middle KD (G, H and I) and high KD groups (J, K and L); (M) Representative images of the spiral ganglion neuron of different experimental groups; (N) Measurement of the height of the organ of Corti in control and different experimental groups; (O) Quantification of spiral ganglion neurons in control and different experimental groups. The red line in panel A indicates the height of the organ of Corti. The scales in panel A and M represent 40 and 30 μm, respectively. # or * $P < 0.05$, significantly different from control group.

low KD group, the mice showed normal hearing for months. Our data suggest that the degree of hearing loss is positively correlated with the level of Cx26 reduction in SCs. Moreover, we speculated that normal expression of cochlear Cx26 would have a certain reserve capacity, and consequently a certain amount of Cx26 reduction in SCs would not result in hearing loss in the low KD group. Our data provides a definite target of gene therapy for *Gjb2*-related hearing loss. If Cx26-based channels could be reconstructed in more than 65% of SCs, deafness could be totally rescued in mouse models. It should be noticed that the Cx26-null SCs are distributed in different types of SCs of the low or middle KD groups. Whether knockout of the *Gjb*2 gene in specific types of SCs can induce hearing loss still requires further study.

Distinct cell degeneration patterns in different experimental groups are due to different levels of residual Cx26 expression. In previous extensive Cx26-null mouse models, knocking out of most of cochlear Cx26 before the opening of TC can induce significant hair cell loss in middle and basal turns (Chang et al., 2015; Chen et al., 2014b; Crispino et al., 2011). Moreover, Lin's group showed that dramatic cell death occurred around P13 in the OHCs and the surrounding SCs in three different extensive Cx26-null lines, in which cochlear Cx26 was knocked out in embryonic stage (Wang et al., 2009). Additionally, in another extensive Cx26-null line, Cohen-Salmon reported that significant hair cell loss was found at P14, soon after the onset of hearing (Cohen-Salmon et al., 2002). Interestingly, it is reported that apoptosis in greater epithelial ridge (GER) persisted until a later stage of cochlear development (P12) in *Gjb2* R75W mutation mouse model, while the number of apoptotic cells in GER decreased from P8 to P12 in control group (Inoshita et al., 2014). In most cases, it seems that this hearing impairment and hair cell loss may occur almost simultaneously when cochlear Cx26 was widely knocked out in embryonic stage. In our study, the similar phenomenon (significant cell degeneration with hearing loss at P20) was also observed in high KD group. However, the hair cell loss occurs much later than the hearing impairment in the middle KD group. This implies that hair cell loss is not a dominant cause of deafness in the middle KD group and other reasons should be carefully considered in this group. Another important finding is that the region and the extent of hair cell loss is quite different between the high KD group and the middle KD group. Although most SCs (> 90%) lost Cx26 expression in the high KD group, severe degeneration of hair cells and neighbouring SCs was only observed in the middle turn at P20. At the same time, a mild degeneration of hair cells was found to occur in the basal turn of this group. These data indicated that the amount of Cx26 expression required to maintain hair cell survival is distinct among different turns. Consequently, ways to induce a high proportion of Cx26-positive SCs in the middle turn of

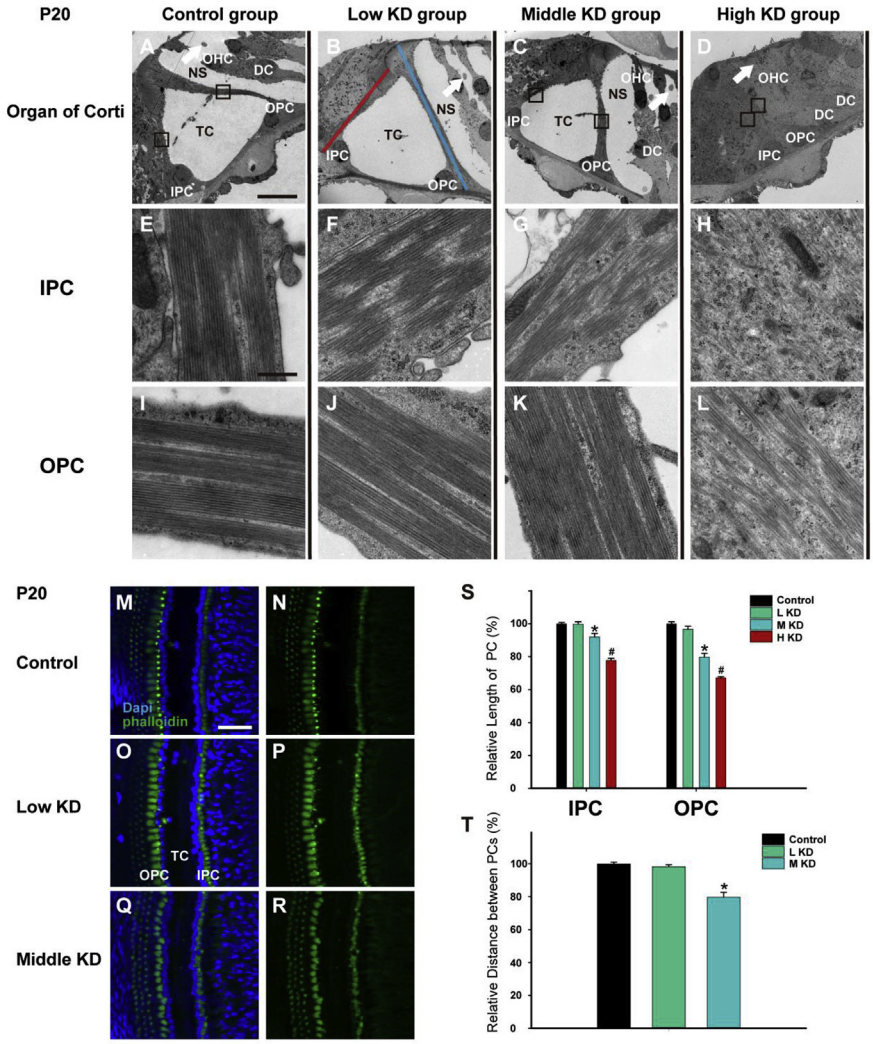

Fig. 5. Ultrastructure of the organs of Corti in control and experimental groups. (A–D) The ultrastructure of organs of Corti in apical turns from control and different experimental groups; The white arrows indicate the phalangeal process of DC, and black boxes (A) are magnified to show the details of PC's (E and I); The red and blue lines in panel B indicate the lengths of IPCs and OPCs, respectively; (E–H) Representative images of the middle part of IPCs in control and different experimental groups; (I–L) Representative images of the middle part of OPCs in control and in different experimental groups; (M–R) Representative images of flattened preparations at PC's level in control (M and N), low KD (O and P) and middle KD group (Q and R). (S) Relative lengths of IPCs and OPCs in control and experimental groups. (T) Relative distance between the nuclei of IPCs and OPCs in control, low KD and middle KD groups. * or #$P < 0.05$, Significantly different from control group. The scales in panel A, E and M represent 20 μm, 500nmand 30 μm, respectively.

an extensive Cx26-null model should be considered preferentially in further treatment studies. Unlike the rapid cell degeneration in the high KD group, late-onset hair cell loss was found in the basal turn of the middle KD group at P60. Considering the relatively small number of OHCs lost in the basal turn, this convinces us that there must be some other causes of the moderate whole-frequency deafness observed in the middle KD group.

Postnatal expression of cochlear Cx26 affects the developmental status of PCs in a dose-dependent manner. In this study, we observed that PCs in the high KD group were in an undifferentiated state. The detailed pathological changes were reported in our previous study (Chen et al., 2018a). Briefly, the presence of undifferentiated IPCs and OPCs at P18–P20 is similar to the juvenile state of PCs (P4–P5) before the opening of the TC, which have fewer intracellular microtubules and stand together. Moreover, these juvenile PCs cause a significant reduction in the height of the organ of Corti, and the adjacent nuclei of IPCs and OPCs caused closure of the TC (Chen et al., 2018a). However, bundles of microtubules were still observed in the PCs, and the TC was able to open up in the middle KD group. Additionally, we found that the height of the organ of Corti was partially reduced and the length of PCs was somewhat reduced. Accordingly, the distances between the nuclei of IPCs and OPCs were also partially reduced. Obviously, the length of microtubules in PCs, but not the density of microtubules, was substantially affected in the middle KD group. PCs are dominated by long bundles of microtubules, and these provide mechanical support for the whole organ of Corti (Tolomeo and Holley, 1997; Zetes et al., 2012). Considering the above findings, we speculated that the decrease in the length of microtubules throughout the body of PCs is responsible for the decrease in PC length. As a result, these shortened PCs are in a developing, or partially-differentiated, state at P20 in the middle KD group. In contrast, the morphology and ultrastructure of PCs are not affected at all in the low KD group. Although scattered Cx26-null PCs were observed in the low KD group, we never observed developing or juvenile PCs in the low KD group. Accordingly, a small proportion of Cx26-null SCs (PC + DC less than 35%) may not affect the developmental process of PCs in the low KD group. In other words, this mosaic deletion pattern will not cause scattered developmental arrest of PCs. In the middle KD group, almost all the PCs were in a partially-differentiated state and the length measurements of these PCs never reached the mean value of those in the control group. This indicated that the status of a single PC is not totally dependent on its own Cx26 expression but instead on the overall level of Cx26 expression by SCs in the cochlear epithelium. In the cochlea, the Cx26-based channels connected adjacent SCs to form a functional syncytium, and this may play an important role in the differentiation of PCs. Different reductions in Cx26 expression may have distinct effects on this syncytium. In the high KD group, up to 90% of SCs lost Cx26 expression and this would totally destroy the function of this syncytium. Because of this, the development of PCs was completely arrested in the high KD group. However, approximately half of SCs still expressed Cx26 in the middle KD group. Consequently, the development of PCs was only delayed or partially arrested in this group. Accordingly, a small reduction of Cx26 expression (less than 35%) in SCs

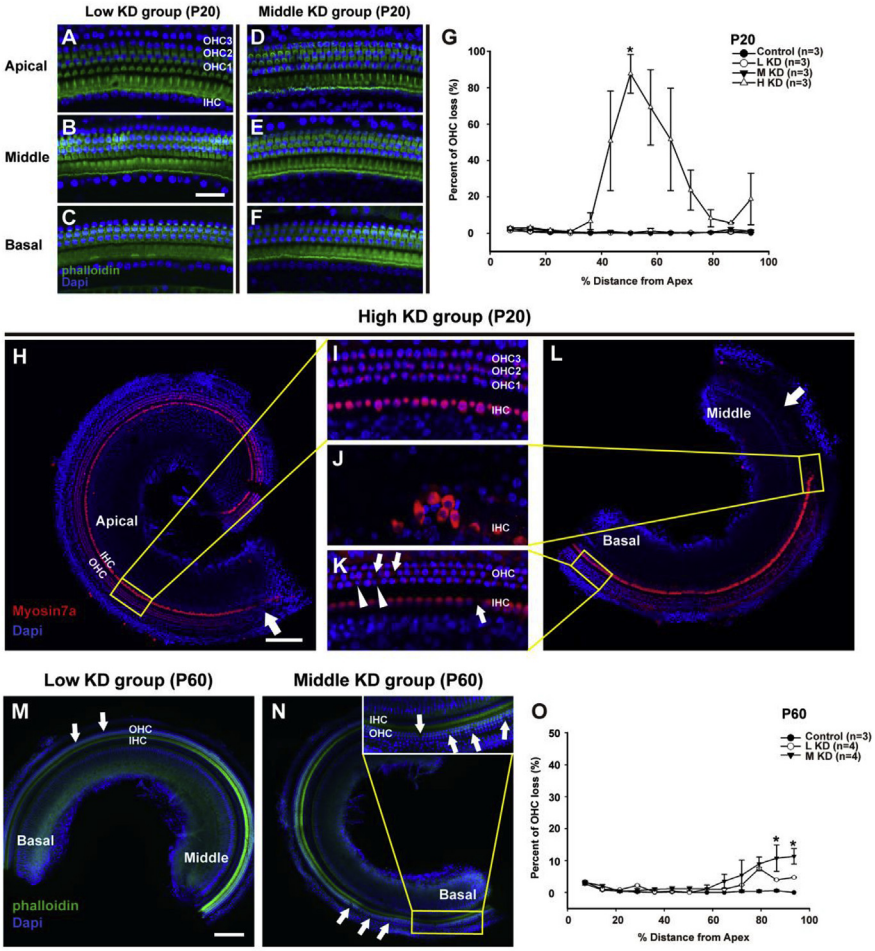

Fig. 6. Patterns and time courses of hair cell loss in the different experimental groups. (A, B and C) Representative images of hair cells in apical (A), middle (B) and basal turns (C) from the low KD group at P20; (D, E and F) Parallel images of hair cells in different turns from the middle KD group at P20; (H) The apical part of the cochlear epithelium in the high KD group at P20; (L) The middle to basal parts of the cochlear epithelium in the high KD group at P20; The yellow boxes in panel H and L are shown magnified in panel I, J and K; Hair cells were stained for myosin7a (red); White arrows indicate the missing hair cells and white arrowheads indicate pyknotic nuclei of hair cells; (G) Quantifications of OHC loss at specific cochlear locations for different groups; (M and N) Representative images of middle to basal parts of the cochlear epithelium in the low KD (M) and middle KD groups (N) at P60. The yellow box in panel N was magnified in the top; White arrows indicate the missing hair cells; (O) Quantifications of OHC loss at specific cochlear locations for low and middle KD groups at P60. The scales in panel B, H and M represent 40, 200 and 200 μm, respectively. $^{*}P < 0.05$, significantly different from control group.

may not affect the developmental process of PCs in the low KD group.

Deformity of PCs may be a potential cause of *Gjb2*-related hearing loss. In previous studies or the high KD group, the cochlear Cx26 was extensively reduced in these models and the severe hair cell loss was observed in middle and basal turns when the ABRs were recorded (Chang et al., 2015; Crispino et al., 2011; Sun et al., 2009). Moreover, a slight reduction of ribbon synapses were found in residual IHC from apical turn in extensive Cx26-null mouse model similar to the high KD group (Chang et al., 2015). The results indicated that the severe hearing loss in extensive Cx26-null models may be due to the sensory hair cell death or the dysfunction of residual hair cells. According to previous studies, Cx26 is expressed in all types of SCs except hair cells (Chen et al., 2018b; Forge et al., 2003; Liu et al., 2009; Sun et al., 2005). Consequently, knockout of the *Gjb2* gene in SCs will primarily cause dysfunction of the SCs. In a mosaic Cx26 KO model, most of DCs and OPCs were knocked out of Cx26, and the DPOAE levels were significantly reduced at high frequency (Lukashkina et al., 2017). It is reported that the late-onset hearing loss of this line was mainly caused by the reduction of active cochlear amplification via the influence nonlinear capacitance of OHCs(Zhu et al., 2013; Zong et al., 2017). However, the DPOAE levels were reduced in all frequency while these was no significant changes in nonlinear capacitance of OHC in a *Gjb2* R75W mutation line. In this report, the author suggested that undifferentiated SCs (malformed organ of Corti similar to that in the high KD group) would impede the cellular function of OHC, which causes the reduction of DPOAEs (Minekawa and Tinoshita, 2009). Moreover, this *Gjb2* R75W mutation can induce macromolecular degradation of large gap junction complexes from the embryonic stage, which was believed to be the primary pathology in mouse (Kamiya et al., 2014). The juvenile PC and severe hearing loss were observed later in this mouse model (Inoshita et al., 2008). In our study, partially-differentiated PCs without hair cell loss were found in the middle KD group. In this group, the number of ribbon synapses in IHC of apical turn is not affected and no significant pathological changes was observed in IHC. The DPOAE levels did not decrease at 8 or 16 kHz either. Although these parameters are far from enough to measure the function of hair cell, it provided an important clue that the hearing loss in the middle KD group can not attributed to the reduction of ribbon synapses in IHC or decreased function of OHC's amplification. These data indicated that developmental abnormalities of PCs may be the primary pathological change rather than an incidental phenomenon in Cx26-null mouse models. Moreover, some studies have reported that *Fgfr*3 regulates the development of PCs. Knockout of the *Fgfr*3 gene in PCs would thus lead to a reduction of microtubules in PCs and hearing loss in mice (Puligilla et al., 2007). These observations proved that malformed PCs can directly cause hearing loss. In our middle and high KD groups, hearing impairment was always accompanied by malformed PCs. However, well-formed PCs were apparent, together with normal hearing, in the low KD group. We speculated that shorter PCs in the middle KD group or juvenile PCs in the high KD group would lead to abnormal mechanical features of the organ of Corti, which may be the cause of hearing loss. However, the specific mechanism involved in deafness still needs further investigation. According to the above findings and speculations, partially-differentiated PCs may be an important cause of hearing loss in the middle KD group. The developmental status of PCs is inversely related to the degree of hearing loss in Cx26-null mouse models.

In conclusion, our data showed that postnatal expression of cochlear

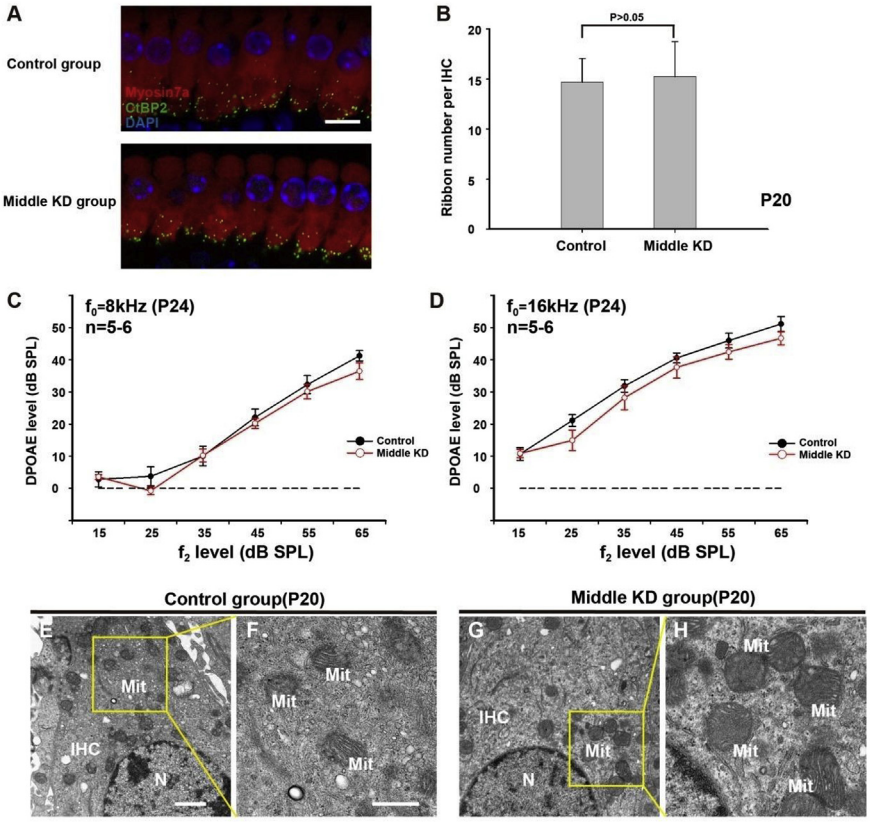

Fig. 7. Ultrastructure of inner hair cell and DPOAE in the middle KD group. (A) Pattern of ribbon synapses (CtBP2, green) in inner hair cell (myosin7a, red) of control and middle KD group; (B) Statistics of the number of ribbon synapses per IHC in apical turn; (C and D) DPAOE levels were measured at P24 and the audiograms were presented at f_0 = 8(C) and f_0 = 16 kHz (D) (f_2/f_1 = 1.2 and the level of f_2 set 10 dB below that of f_1). The dashed line indicates noise floor. (E and G) Representative ultrastructural images of IHC from control (E) and the middle KD group (G). The yellow boxes in panel E and G was shown magnified in panel F and H. N: nuleus; Mit: mitochondria; IHC, inner hair cell. The scales in panel A, E and F represent 5 μm, 1 μm and 500 nm, respectively.

Cx26 can induce hearing loss in a dose-dependent manner. For a single PC, the developmental status is not fully dependent on its own Cx26 expression. The overall level of cochlear Cx26 may affect the developmental status of PCs in a dose-dependent manner. Hair loss is not a dominant cause of hearing loss in a partial Cx26-null model. Deformity of PCs may also be a potential cause of *Gjb2*-related hearing loss.

4. Materials and methods

4.1. Mouse models

$Cx26^{loxP/loxP}$ mice and Rosa26CreER mice were provided by Prof. Xi Lin at Emory University. Tamoxifen-inducible $Cx26^{loxP/loxP}$;Rosa26CreER mice were generated by crossbreeding the $Cx26^{loxP/loxP}$ mice with the Rosa26CreER mice. Mouse genotyping was performed by PCR amplification of tail genomic DNA. Details of the mice were given in our previous paper (Sun et al., 2009; Zhou et al., 2016). The genotyping primers were as follows:

Cx26(F):5′-ACAGAAATGTGTTGGTGATGG-3′, Cx26(R):5′-CTTTCCAATGCTGGTGGAGTG-3′, Rosa26Cre(F):5′-AGCTAAACATGCTTCATCGTCGGTC-3′, Rosa26Cre(R):5′-TATCCAGGTTACGGATATAGTTCATG-3'.

It has been reported that CreER activation is TMX dose-dependent (Erdmann et al., 2007; Hayashi and McMahon, 2002; McGovern et al., 2017; Zhong et al., 2015). To obtain mice with different degrees of Cx26 deficiency, different doses of TMX (T5648-1G, Sigma-Aldrich, St Louis, MO, USA) (1.6 mg/10g, 1.1 mg/10g or 0.6 mg/10g body weight) were injected subcutaneously at P0. $Cx26^{loxP/loxP}$;Rosa26CreER mice were used in experimental groups, while the littermates without Cre were used as controls.

All mice were raised in the specific-pathogen-free Experimental Animal Centre of Huazhong University of Science and Technology. All efforts were made to minimize animal suffering, to reduce the number of animals used. All experimental procedures were conducted in accordance with the policies of the Committee on Animal Research of Tongji Medical College, Huazhong University of Science and Technology.

4.2. Auditory brainstem response (ABR) and distortion product otoacoustic emission (DPOAE)

ABR was measured at P20 or P60. As we previously reported, mice (n = 5–9 mice in each group) were anaesthetized by intraperitoneal injection with a mixture of ketamine (120 mg/kg) and chlorpromazine (20 mg/kg). Body temperature was maintained by placing anaesthetized mice on a heating pad. The recording electrode was placed at the vertex, and the reference electrode was inserted into the tested ear with a ground electrode at the contralateral ear. Tone bursts of various frequencies (4, 8, 16 and 32 kHz) were generated and responses were recorded using the Tucker-Davis Technologies System (RZ6, Tucker-Davis Tech. Inc., Alachua, FL, USA). The responses were averaged 1,024 times and recorded in decreasing 10 dB steps, narrowing to 5 dB steps near the threshold. The ABR threshold at each frequency was determined by the lowest sound level that could be recognized. To measure DPOAE (n = 5–6mice in each group), the frequency was presented by a geometric mean of f_1 and f_2 [$f_0 = (f_1 \times f_2)^{1/2}$] with a ratio of f_1:f_2 = 1:1.2. The level of f_2 tone was set 10 dB below that of f_1 tone. The distortion product was recorded with average of 200 times. The $2f_1$-f_2 component was measured.

4.3. Protein extraction and western blotting

Mice were deeply anaesthetized and sacrificed at P7. Mouse cochleae were carefully dissected from the temporal bones in ice cold 0.01M phosphate-buffered saline (PBS) and were pooled (4 mice in each group, three experiments were repeated). The total proteins of membranous labyrinth were extracted using RIPA lysis buffer (P0013B, Beyotime Institute of Biotechnology, Jiangsu, PRC). Protein concentrations were quantified using a bicinchoninic acid protein assay kit

(P0012S, Beyotime Biotechnology). Equal amounts of protein samples (10 μg per lane) were separated by electrophoresis on 12% SDS-PAGE gels and then transferred to polyvinylidenedifluoride (PVDF) membranes. The membranes were blocked in TBST (Tris-buffered saline with 0.1% Tween 20) containing 5% milk for 1 h Cx26 and β-actin proteins were detected using rabbit polyclonal antibodies against Cx26 (1:1,000 dilution, 512800, Invitrogen, Carlsbad, CA, USA) or rabbit polyclonal antibodies against β-actin (1:1,000 dilution, 04–1116, Merck-Millipore, Darmstadt, Germany). After washing in TBST, bands were incubated with horseradish peroxidase (HRP)-conjugated goat anti-rabbit secondary antibody for 1 hat room temperature. Bands were visualized with an ECL reaction kit (P0018, Beyotime Biotechnology). The protein levels of Cx26 were measured using Quantity One 4.6.2 (Bio-Rad, Hercules, CA, USA) and were normalised to the levels of β-actin in the corresponding lane.

4.4. Cochlear tissue preparation and immunofluorescent labelling

For frozen sections, the temporal bones were harvested and dissected at P7 then fixed in 4% paraformaldehyde in PBS for 1 h at room temperature. After decalcification with disodium EDTA for 48 h, the cochleae were dehydrated with 20% and 30% sucrose for 1.5 h and embedded in OCT. Modiolar sections with a thickness of 10 μm were cut for subsequent procedures. For Cx26-null cell quantification, mice (n = 3–5 mice in each group) were deeply anaesthetized and sacrificed at P7. For cochlear hair cell and SC counts, mice (n = 3–4 in each group) were sacrificed at P20 and P60. The cochleae were fixed in 4% paraformaldehyde in 0.01M PBS for 1 hat room temperature. Each stretched cochlear preparation was carefully dissected in ice-cold 0.01M PBS. After blocking in 10% donkey serum with 1% Triton X-100 for 1 h, the samples were then incubated with polyclonal rabbit anti-Cx26 antibodies (1:200 dilution, 512800, Invitrogen), mouse IgG_1 anti-CtBP2 (1:100, 612044, BD Biosciences) or polyclonal rabbit anti-myosin7a antibody (1:500 dilution, 25–6790, Proteus Bio-Sciences, Ramona, CA, USA) diluted in 0.01M PBS with 0.3% Triton X-100 overnight at 4 °C. Samples were washed three times in 0.01 M PBS with 0.1% Tween-20 and then stained by Alexa Fluor 647-conjugated donkey anti-rabbit IgG (1:200 dilution, ANT032, Antgene Biotechnology Company Ltd, Wuhan, PRC) for 1.5 h. DAPI (C1005, Beyotime Biotechnology) and phalloidin (0.05 mg/mL, P5282, Sigma) were used for nuclear and F-actin staining, respectively. Images were captured with a laser scanning confocal microscope (Nikon, Tokyo, Japan).

For Cx26-null cell quantification, three regions from the apical, middle, and basal turns of the stretched cochlear preparation were scanned by × 60 magnification lens. A total number of approximate 500 SCs from one mouse were taken into counting (3–5 mice in each group). The same manner was performed for SC counts (n = 3–4 mice in each group). To better understand residual Cx26 expression in SCs, images from different levels of SCs were merged together. For hair cell counts, the whole stretched cochlear preparation were captured by × 10 magnification lens. To get the cochleograms, about 2100 outer hair cells in each sample were counted in 13 consecutive fields from the apical to the basal portion. The last part of the basilar membrane of cochlea was anfractuous and hard to obtain, so the counted parts covered nearly 94 percents of the whole basilar membrane (n = 3–4 mice in each group). The distance between the nuclei of the IPCs and OPCs (30 pairs of IPCs and OPCs from 3 mice in each group) was measured at P20 using Image-Pro Plus 6.0.

4.5. Resin sections and transmission electron microscopy (TEM)

Mice were deeply anaesthetized and sacrificed at P20. The cochleae were removed and fully fixed with a mixture of 2% paraformaldehyde and 2.5% glutaraldehyde in 0.1M PB. The samples were decalcified for 48–72 h in 10% disodium EDTA (pH = 7.2) and post-fixed for 1 h in 1% osmium tetroxide. After dehydration through a graded ethanol series, samples were embedded in resin. The samples were sectioned (1.5 μm in thickness) and stained with toluidine blue (89640-5G, Sigma-Aldrich) for light microscope observation (9-12 sections from 3 to 4 mice in each group). The distances from the top of head conjunction of the IPCs and OPCs to the basilar membrane were measured using Image-Pro Plus 6.0. To evaluate of the number of spiral ganglion neurons, neighbouring sections separated by 40 μm were used to avoid double counting. The area of the Rosenthal's canal was measured with Image Pro Plus 6.0 from these sections, and the neurons with distinct nucleus were taken into counting.

Ultrathin sections (80 nm in thickness) in were stained with uranyl acetate and lead citrate for electron microscopic examination (FEI Tecnai G2 20 TWIN, Thermo Fisher Scientific, Waltham, MA, USA). The lengths of the IPCs and OPCs (9-12 sections from 3 to 4 mice in each group) were measured as shown in Fig. 5 B using Image-Pro Plus 6.0. The measurement line is parallel to the long axis of pillar cells.

4.6. Statistical analysis

All data are presented as means ± s.e.m. and plotted by Sigma Plot (Version 12.5 Systat Software, Inc., San Jose, CA, USA). The One-way analysis of variance (ANOVA) and the least significant difference (LSD) post hoc test or unpaired *t*-test were performed using SPSS software (version 19, IBM SPSS Statistics, Armonk, NY, USA), and $P < 0.05$ was considered to be statistically significant.

Author contributions statement

YS and WK conceived and designed the experiments; LX, SC, KX and AD performed the experiments; HC and SC analyzed the data; XB and KX contributed the mouse breeding; YS and SC wrote the paper.

Conflicts of interest statement

No competing interests declared.

Funding

The work was supported by grants from The National Natural Science Foundation of China(No. 81470696, 81771003, 81500793, and 81570923).

Acknowledgments

We would like to thank the Centre for Instrumental Analysis and Metrology, Institute of Virology, Chinese Academy of Science, for our Electron Microscopy (EM) and we would be grateful to Ding Gao, Pei Zhang and Bi-Chao Xu for their help of EM experiments.

Abbreviations

Cx26	Connexin26
HC	hair cell
PC	pillar cell
KD	knockdown
SC	supporting cell
TC	tunnel of Corti
SNHL	sensorineural hearing loss
DC	Deiter's cell
TMX	tamoxifen
NS	Nuel's space
ABRs	auditory brainstem responses
DPOAE	distortion product otoacoustic emission

References

Azaiez, H., Chamberlin, G.P., Fischer, S.M., Welp, C.L., Prasad, S.D., Taggart, R.T., Del, C.I., Van, C.G., Smith, R.J., 2010. GJB2: the spectrum of deafness-causing allele variants and their phenotype. Hum. Mutat. 24, 305–311.

Chan, D.K., Chang, K.W., 2014. GJB2-associated hearing loss: systematic review of worldwide prevalence, genotype, and auditory phenotype. Laryngoscope 124, E34–E53.

Chang, Q., Tang, W., Kim, Y., Lin, X., 2015. Timed conditional null of connexin26 in mice reveals temporary requirements of connexin26 in key cochlear developmental events before the onset of hearing. Neurobiol. Dis. 73, 418–427.

Chen, J., Chen, J., Zhu, Y., Liang, C., Zhao, H.B., 2014a. Deafness induced by Connexin 26 (GJB2) deficiency is not determined by endocochlear potential (EP) reduction but is associated with cochlear developmental disorders. Biochem. Biophys. Res. Commun. 448, 28–32.

Chen, S., Sun, Y., Lin, X., Kong, W.J., 2014b. Down regulated connexin26 at different postnatal stage displayed different types of cellular degeneration and formation of organ of Corti. Biochem. Biophys. Res. Commun. 445, 71–77.

Chen, S., Xie, L., Xu, K., Cao, H.Y., Wu, X., Xu, X.X., Sun, Y., Kong, W.J., 2018a. Developmental abnormalities in supporting cell phalangeal processes and cytoskeleton in the Gjb2 knockdown mouse model. Dis. Model Mech. 11.

Chen, S., Xu, K., Xie, L., Cao, H.Y., Wu, X., Du, A.N., He, Z.H., Lin, X., Sun, Y., Kong, W.J., 2018b. The spatial distribution pattern of Connexin26 expression in supporting cells and its role in outer hair cell survival. Cell Death Dis. 9.

Cohen-Salmon, M., Ott, T., Michel, V., Hardelin, J.P., Perfettini, I., Eybalin, M., Wu, T., Marcus, D.C., Wangemann, P., Willecke, K., Petit, C., 2002. Targeted ablation of connexin26 in the inner ear epithelial gap junction network causes hearing impairment and cell death. Curr. Biol. 12, 1106–1111.

Crispino, G., Di Pasquale, G., Scimemi, P., Rodriguez, L., Galindo Ramirez, F., De Siati, R.D., Santarelli, R.M., Arslan, E., Bortolozzi, M., Chiorini, J.A., Mammano, F., 2011. BAAV mediated GJB2 gene transfer restores gap junction coupling in cochlear organotypic cultures from deaf Cx26Sox10Cre mice. PLoS One 6 e23279.

Erdmann, G., Schutz, G., Berger, S., 2007. Inducible gene inactivation in neurons of the adult mouse forebrain. BMC Neurosci. 8, 63.

Forge, A., Becker, D., Casalotti, S., Edwards, J., Marziano, N., Nevill, G., 2003. Gap junctions in the inner ear: comparison of distribution patterns in different vertebrates and assessement of connexin composition in mammals. J. Comp. Neurol. 467, 207–231.

Gazzaz, B., Weil, D., Rais, L., Akhyat, O., Azeddoug, H., Nadifi, S., 2005. Autosomal recessive and sporadic deafness in Morocco: high frequency of the 35delG GJB2 mutation and absence of the 342-kb GJB6 variant. Hear. Res. 210, 80–84.

Harris, A.L., 2001. Emerging issues of connexin channels: biophysics fills the gap. Q. Rev. Biophys. 34 325-472.

Hayashi, S., McMahon, A.P., 2002. Efficient recombination in diverse tissues by a tamoxifen-inducible form of Cre: a tool for temporally regulated gene activation/inactivation in the mouse. Dev. Biol. 244, 305–318.

Iizuka, T., Kamiya, K., Gotoh, S., Sugitani, Y., Suzuki, M., Noda, T., Minowa, O., Ikeda, K., 2015. Perinatal Gjb2 gene transfer rescues hearing in a mouse model of hereditary deafness. Hum. Mol. Genet. 24, 3651–3661.

Inoshita, A., Iizuka, T., Okamura, H.O., Minekawa, A., Kojima, K., Furukawa, M., Kusunoki, T., Ikeda, K., 2008. Postnatal development of the organ of Corti in dominant-negative Gjb2 transgenic mice. Neuroscience 156, 1039–1047.

Inoshita, A., Karasawa, K., Funakubo, M., Miwa, A., Ikeda, K., Kamiya, K., 2014. Dominant negative connexin26 mutation R75W causing severe hearing loss influences normal programmed cell death in postnatal organ of Corti. BMC Genet. 15, 1.

Jagger, D.J., Forge, A., 2015. Connexins and gap junctions in the inner ear–it's not just about K(+) recycling. Cell Tissue Res. 360, 633–644.

Centers for disease control and prevention. National center on birth defects and developmental disabilities. Hear. Loss. http://www.cdc.gov/ncbddd/dd/ddhi.htm.

Kamiya, K., Yum, S.W., Kurebayashi, N., Muraki, M., Ogawa, K., Karasawa, K., Miwa, A., Guo, X., Gotoh, S., Sugitani, Y., Yamanaka, H., Ito-Kawashima, S., Iizuka, T., Sakurai, T., Noda, T., Minowa, O., Ikeda, K., 2014. Assembly of the cochlear gap junction macromolecular complex requires connexin 26. J. Clin. Investig. 124, 1598–1607.

Liu, Y., Ke, X., Qi, Y., Li, W., Zhu, P., 2002. Connexin26 gene (GJB2): prevalence of mutations in the Chinese population. J. Hum. Genet. 47, 688–690.

Liu, W., Bostrom, M., Kinnefors, A., Rask-Andersen, H., 2009. Unique expression of connexins in the human cochlea. Hear. Res. 250, 55–62.

Lukashkina, V.A., Yamashita, T., Zuo, J., Lukashkin, A.N., Russell, I.J., 2017. Amplification mode differs along the length of the mouse cochlea as revealed by connexin 26 deletion from specific gap junctions. Sci. Rep. 7.

McGovern, M.M., Brancheck, J., Grant, A.C., Graves, K.A., Cox, B.C., 2017. Quantitative analysis of supporting cell subtype labeling among CreER lines in the neonatal mouse cochlea. J. Assoc. Res. Otolaryngol. 18, 227–245.

Minekawa, A., Tinoshita, A., 2009. Cochlear outer hair cells in a dominant-negative connexin26 mutant mouse preserve non-linear capacitance in spite of impaired distortion product otoacoustic emission. Neuroscience 164, 1312.

Puligilla, C., Feng, F., Ishikawa, K., Bertuzzi, S., Dabdoub, A., Griffith, A.J., Fritzsch, B., Kelley, M.W., 2007. Disruption of fibroblast growth factor receptor 3 signaling results in defects in cellular differentiation, neuronal patterning, and hearing impairment. Dev. Dynam. 236, 1905–1917.

Rabionet, R., Zelante, L., Lopez-Bigas, N., D'Agruma, L., Melchionda, S., Restagno, G., Arbones, M.L., Gasparini, P., Estivill, X., 2000. Molecular basis of childhood deafness resulting from mutations in the GJB2 (connexin 26) gene. Hum. Genet. 106, 40–44.

Rennels, M., Pickering, L.K., 2005. Sensorineural hearing loss in children. Lancet 365, 2085–2086.

Sun, J., Ahmad, S., Chen, S., Tang, W., Zhang, Y., Chen, P., Lin, X., 2005. Cochlear gap junctions coassembled from Cx26 and 30 show faster intercellular Ca2+ signaling than homomeric counterparts. Am. J. Physiol. Cell Physiol. 288, C613–C623.

Sun, Y., Tang, W., Chang, Q., Wang, Y., Kong, W., Lin, X., 2009. Connexin30 null and conditional connexin26 null mice display distinct pattern and time course of cellular degeneration in the cochlea. J. Comp. Neurol. 516, 569–579.

Tolomeo, J.A., Holley, M.C., 1997. Mechanics of microtubule bundles in pillar cells from the inner ear. Biophys. J. 73, 2241–2247.

Tsukada, K., Nishio, S., Usami, S., 2010. A large cohort study of GJB2 mutations in Japanese hearing loss patients. Clin. Genet. 78, 464–470.

Wang, Y., Chang, Q., Tang, W., Sun, Y., Zhou, B., Li, H., Lin, X., 2009. Targeted connexin26 ablation arrests postnatal development of the organ of Corti. Biochem. Biophys. Res. Commun. 385, 33–37.

Yu, Q., Wang, Y., Chang, Q., Wang, J., Gong, S., Li, H., Lin, X., 2014. Virally expressed connexin26 restores gap junction function in the cochlea of conditional Gjb2 knockout mice. Gene Ther. 21, 71–80.

Zetes, D.E., Tolomeo, J.A., Holley, M.C., 2012. Structure and mechanics of supporting cells in the Guinea pig organ of Corti. PLoS One 7 e49338.

Zhang, Y., Tang, W., Ahmad, S., Sipp, J.A., Chen, P., Lin, X., 2005. Gap junction-mediated intercellular biochemical coupling in cochlear supporting cells is required for normal cochlear functions. Proc. Natl. Acad. Sci. U. S. A. 102, 15201.

Zhong, Z.A., Sun, W., Chen, H., Zhang, H., Lay, Y.E., Lane, N.E., Yao, W., 2015. Optimizing tamoxifen-inducible Cre/loxp system to reduce tamoxifen effect on bone turnover in long bones of young mice. Bone 81, 614–619.

Zhou, X.X., Chen, S., Xie, L., Ji, Y.Z., Wu, X., Wang, W.W., Yang, Q., Yu, J.T., Sun, Y., Lin, X., Kong, W.J., 2016. Reduced Connexin26 in the mature cochlea increases susceptibility to noise-induced hearing loss in mice. Int. J. Mol. Sci. 17.

Zhu, Y., Liang, C., Chen, J., Zong, L., Chen, G.D., Zhao, H.B., 2013. Active cochlear amplification is dependent on supporting cell gap junctions. Nat. Commun. 4 1786-1786.

Zong, L., Chen, J., Zhu, Y., Zhao, H.B., 2017. Progressive age-dependence and frequency difference in the effect of gap junctions on active cochlear amplification and hearing. Biochem. Biophys. Res. Commun. 489 S0006291X17310379.